Research on Dynamic Response Characteristics of a New Integrated System with Multiple Wind Turbines

Jiangfeng Zhu[1*], Qian Zhao[2]
[1] College of Intelligent Manufacturing, Qingdao Huanghai University, Qingdao, 266427, China.
[2] College of Mechanical Engineering, Ocean University of China, Ltd, Qingdao, 266580, China.

* Corresponding author. Email: z6j2f8@163.com (J.Z.); zhu0055@126.com (Q.Z.)
Manuscript submitted December 30, 2025; accepted January 9, 2026; published April 23, 2026.
doi: 10.12720/sgce.15.1.15-30

Abstract: This study introduces an innovative concept that integrates offshore floating wind turbines with aquaculture cages, termed the Dot Matrix Floating (DMF) integration system for new offshore fisheries. To evaluate the safety and hydrodynamic operational adaptability of the overall DMF structural system, the investigation was conducted through three primary approaches: structural strength reliability analysis, numerical simulation of hydrodynamic responses, and small-scale prototype flume experiments. Initially, a multi-wind turbine wake model was developed, and fluid-structure interaction simulations were employed to characterize the variation patterns of multi-wind load wakes within the DMF structure. Subsequently, the validity of the hydrodynamic response simulations was confirmed by comparing numerical results with experimental data obtained from wave-current flume tests. Additionally, by examining the hydrodynamic response behaviors of the DMF under various mooring configurations, the study identified an optimal mooring strategy suitable for multi-wind turbine integrated systems. Finite element analysis further demonstrated that the overall structural stresses remain within acceptable safety limits. Ultimately, through the combined application of DMF modeling and finite element numerical simulations, an integrated analytical framework encompassing aerodynamics, hydrodynamics, and structural mechanics for multiple wind turbines was established. This framework offers valuable guidance and a reference point for addressing critical mechanical challenges in the development of novel floating offshore equipment.

Keywords: fishery wind power integration, strength analysis, dynamic response, flume test, reliability

1. Introduction

The ocean energy sector has experienced significant global expansion due to its abundant resources, stable wind conditions, environmental sustainability, and various other benefits. To enhance the development potential of deep and open sea areas, maximize the economic advantages of offshore wind power and aquaculture industries, reduce costs, and improve the overall efficiency of marine spatial energy utilization, this study proposes a novel integrated development model combining offshore wind power and cage aquaculture. A new marine fishery-power integration system is designed and developed, with an emphasis on its safety and reliability.

Specifically, multiple NREL baseline 5 MW wind turbines are integrated with hexagonal aquaculture cages to achieve combined wind power generation and fishery aquaculture functions. From a construction cost perspective, the wind turbines and aquaculture cages share a semi-submersible buoy and mooring lines, which reduces expenses, facilitates installation, and promotes efficient three-dimensional utilization of marine space. Regarding load conditions, offshore wind turbines are predominantly influenced by wind forces, which can induce significant tilt moments on the tower. Conversely, aquaculture cages primarily

experience wave and current forces, resulting in substantial motion responses in sway, heave, and other degrees of freedom. The proposed fishery-power structure is subjected to considerable wind loads above the water surface and wave and current loads below, necessitating a comprehensive analysis of the combined effects of wind, wave, and current on the hydrodynamic stability of the integrated system.

Previous studies have addressed related topics: Liang [1] designed a square cage floating frame system and conducted hydrodynamic analyses, though its stability was inferior to that of circular and hexagonal cages. Wang [2] introduced a composite floating photovoltaic and aquaculture device integrated with offshore wind turbines but did not investigate structural strength or stability in detail. Jiang [3] examined the design and mechanical properties of breeding cages installed on jacket wind turbine foundations, identifying limitations in single-support wind turbine structures. Wang [4] analyzed numerous floating wind turbine systems, including the OC3 Hywind [5] spar float equipped with the NREL 5 MW turbine, concluding that platforms with catenary mooring systems exhibit significant pitch motions under typical wave frequencies.

This research builds upon these foundations to develop a robust, cost-effective, and efficient integrated offshore wind power and aquaculture system, addressing both structural and environmental challenges inherent in marine energy utilization.

Under rated load conditions, the pitch motion amplitude attains 8°, whereas under extreme load conditions, it increases to 14°. These findings confirm that the pitch response of floating wind turbines is significantly influenced by the combined effects of wind, wave, and current forces. Sandner's 1:60 scale model test of the semi-submersible platform, utilized in the OC4 DeepCwind project, was conducted at the testing pool of the Centrale Nantes Polytechnic University in France. A ducted wind turbine model equipped with feedback control was employed to simulate the aerodynamic load effects on the six degree of freedom motion response of offshore wind power generation platform. Chen [6] studied the influence of wave motion on the wind and aerodynamic effects of floating structures based on the wake section method. In the present study, we analyzed the structural strength and hydrodynamic response characteristics of the designed integrated fishery power device by comparing finite element hydrodynamic numerical simulation with wave channel experiments. These are of great significance for the study of structural safety and floating stability in nearshore environments.

The DMF concept introduced herein exhibits notable novelty in both structural configuration and dynamic response characteristics when compared to existing integrated offshore wind-aquaculture platforms [7]. Structurally, most current integrated platforms consist of either single wind turbines or dual wind turbine arrangements. In contrast, the DMF presented in this study features a symmetrical layout of six wind turbines. For example, the "Guoneng Shared Number" platform [8], a three-column semi-submersible structure developed in China in 2025, combines single wind turbines with aquaculture cages. Similarly, the European W2Power system [9–11] integrates intelligent net cages with a parallel dual wind turbine configuration. Compared to these existing systems, the DMF employs a hexagonal net cage design and a symmetrical distribution of six wind turbines, enhancing stability and enabling more effective adaptation to multidirectional wind, wave, and current loads across 360 degrees, thereby improving operational reliability.

Regarding dynamic response characteristics, the wind turbines within the DMF are arranged in three rows—front, middle, and rear. Consequently, the wake effects generated by the front row turbines exert a considerable influence on the power generation efficiency and dynamic stability of the turbines positioned in the middle and rear rows.

1.1. Design and Analysis of New DMF Integrated Infrastructure

1.1.1. Main structure scheme design

This study proposes a novel integrated configuration for combined fishery and wind power systems,

characterized by an "upper wind turbine, middle cage, and lower pontoon" arrangement. The wind turbines employed correspond to the 5 MW model parameters published by the National Renewable Energy Laboratory (NREL) [12]. Six units are symmetrically positioned to ensure the floating stability of the entire assembly in the marine environment. The minimum spacing between adjacent turbine towers is maintained at 1.5 times the rotor diameter (1.5D), with the rotor diameter carefully selected to minimize aerodynamic interference and optimize power generation efficiency, thereby achieving a total wind power capacity of 30 MW. The intermediate fishery net cage adopts a hexagonal design, which offers favorable structural integrity and hydrodynamic stability. The netting is fully enclosed, enabling the cage to operate in both fully submerged and semi-submersible modes, thereby enhancing resilience against extreme wind and wave conditions. Drawing on the structural features of the OC4 and WindFloat [13–15] semi-submersible platforms, the lower pontoons interconnect six main pontoons into the hexagonal cage framework via cross bracing. The mooring system utilizes a three-point catenary configuration. The detailed structural layout is illustrated in Fig. 1. The integrated interaction among the wind turbines, fishery cage, and pontoon foundation effectively enhances the overall structural safety of the combined fishery and wind power system, while mitigating the risks of stress concentration and tilt-induced drift failures.

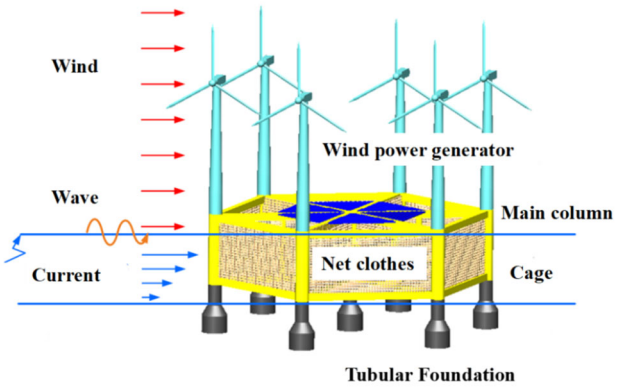

Fig. 1. Concept of DMF overall scheme.

The DMF key structure design is shown in Table 1. The DMF is designed as a floating structure, with an operational water depth of 100 meters selected to accommodate the requirements of deep and offshore floating equipment development. The parameters for the NREL [16] baseline 5 MW wind turbine generator are adopted in accordance with the NREL design specifications. The hexagonal cage platform primarily comprises the main pontoon, water pressure cylinders, and cross braces. The design principle ensures that the buoyancy generated by the pontoon exceeds the combined weight of the six wind turbines and the cage structure.

Table 1. DMF key structural parameters

Items	Parameters	results
Wind power system	Equivalent center of gravity coordinates/m	(−0.2, 0.0, 64.0)
	Wind wheel	Windward, three blades
	Water height, sweeping radius/m	120,59
	Starting, rated, maximum speed/m/s	3, 11.4, 25
Fishery aquaculture platform system	Waterline surface, water depth/m	35,100
	Total length/m	354
	Pontoon height, diameter/m	40,25
	Center of gravity coordinates/m	0,0,−16.8
	I_{xx}, I_{yy}, I_{zz}/m^4	9.788×10^{12}, 9.788×10^{12}, 4.089×10^{12}
	Total weight/kg	4.35×10^{8}
	Length of single mooring line/m	216
	Single anchor mass/kg	1053.2

1.1.2. Environmental load analysis

(1) Wind load

The impact of wind loading on the DMF cannot be overlooked. This study focuses on examining the the impact of aerodynamic loads on the dynamic response stability and structural safety of DMF platforms. Utilizing Jensen's [17–19] single wind turbine wake theory as a foundation, a multi-turbine wake mechanics analysis model is developed, which accounts for the influence of wakes from multiple upstream turbines on downstream units. Fig. 2 is provided below to illustrate this model.

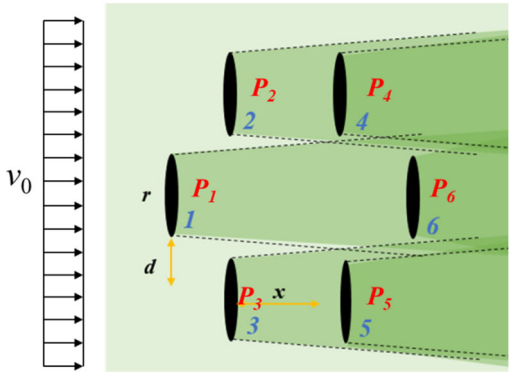

Fig. 2. Multiple wind turbine wake.

As illustrated in Fig. 2, the P6 wind turbine is concurrently influenced by the wake effects generated by the P1 and T4 wind turbines. Several computational approaches exist to assess the impact of multiple wake interactions, including: Eq. (1) geometric methods, Eq. (2) linear summation, Eq. (3) energy balance techniques, and Eq. (4) the sum of squares method. Typically, the wake effects are combined using the sum of squares approach. The downstream wind velocity can be determined accordingly.

$$v_n = \left[1 - \sqrt{\sum_{i=1}^{n} w_{ij}^2}\right] v_0 \tag{1}$$

In the formula, *J* are all possible positions of the wind turbine. w_{ij}^2 is the wake influence factor of wind turbine *J*.

$$w_{ij}^2 = \frac{\left(1 - \sqrt{1 - C_T}\right) r_0^2}{\left(r_0^2 + a x_{ij}\right)^2} \tag{2}$$

Considering the hydrodynamic six-degree-of-freedom oscillatory behavior of the wind turbine system, the turbine's orientation undergoes changes, as depicted in Fig. 3.

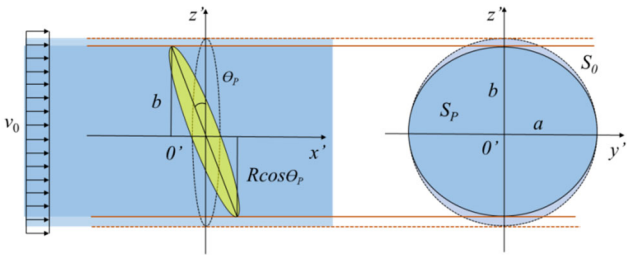

Fig. 3. Wind turbine inclined wind area wake.

When subjected to wave and current forces in the marine environment, the wind turbine foundation experiences vibrational responses, resulting in continuous variations in the windward area of the rotor. Consequently, the wind-driven rotor disk exhibits roll motion, deforming from a circular to an elliptical shape. This deformation pattern is presented in Fig. 3, where the windward area S_P is characterized by the following relationship:

$$S_P = \pi ab = \pi R^2 \cos\theta_P \tag{3}$$

Drawing upon the principles governing six degrees of freedom motion, Fig. 4 illustrates the overall variation in the windward surface area of the wind turbine rotor subjected to the superimposed motion response.

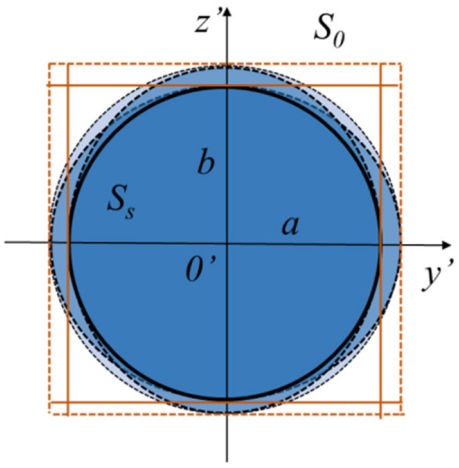

Fig. 4. Multi degree of freedom overlay area.

The overall windward area meets the following requirements (Fig. 5):

$$S_S = \pi ab = \pi R^2 \cos\theta_P \cos\theta_Y \tag{4}$$

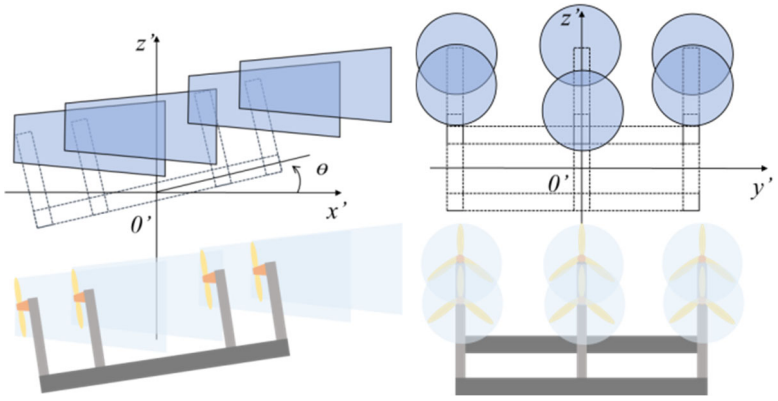

Fig. 5. Multi wind turbine roll motion wake.

(2) Wind, wave and current load

The methodology for calculating wind, wave, and current frequency loads is grounded in the characteristic member section λ ratio, which pertains to small-scale components $D(D/\lambda \le 0.2)$. Utilizing Morison's [20]

equation, the wind, wave, and current frequency loads acting on structural elements such as netting and minor components within this study are determined accordingly.

Because DMF is semi submersible and has a small underwater size, the flow load can be simplified to a constant velocity. Calculation meets:

$$F = F_D + F_I \tag{8}$$

where $F_D = \frac{1}{2}\rho_w C_D D\left|u-\dot{x}\right|\left(u-\dot{x}\right)$ is the ocean current load. $F_I = \frac{\pi}{4}\rho_w C_I D^2\left(C_m\dot{u}-C_A\ddot{x}\right)$ is an inertial load on water. C_D s the drag coefficient of ocean currents. C_I is the inertia force coefficient of waves. u is the normal wave velocity. x is the tangential wave velocity. $D(D/\lambda \le 0.2)$ is a large-span floating system on the sea, which generally bears inertia force and flow force. The calculation of wind, wave and current load conforms to the three-dimensional potential flow theory.

$$F_K = \frac{1}{2}\left(C_{dn}\cos a + C_{dt}\sin a\right)\rho_w l d V_0^2 + C_M \rho V \frac{\partial v}{\partial t}\cos a \tag{9}$$

C_{dn} is the normal drag coefficient. C_{dt} is a tangential coefficient. C_M is the mass ratio coefficient of water.

(3) Current load

The ocean current load is simplified to a constant state. Calculation meets:

$$F_C = \frac{\rho}{2} A C_{DC} V_{RC}^2 \tag{10}$$

C_{DC} is the normal coefficient. $V_{RC} = V_C - V_S$ is the relative velocity of DMF in the horizontal direction. V_C is the true flow rate of DMF.

1.1.3. Phase angle search maximum environmental load

The wave phase angles of the Dynamic Motion Forces (DMF) induced by waves approaching from varying directions differ significantly, leading to distinctly different the hydrodynamic load applied on the DMF platform. Prior to conducting static analysis, it is crucial to determine the maximum wave load applied to the DMF underwater structure. The net enclosure is configured as a regular hexagon centered on the structure. For the purposes of this analysis, only waves with incident angles of 0°, 15°, and 30° are considered. For each wave incident direction, the wave phase angle is varied systematically from 0° to 360°, enabling the identification of the maximum wave-current coupling force and its corresponding phase angle relationship curve. Fig. 6 illustrates the maximum wave phase angle obtained.

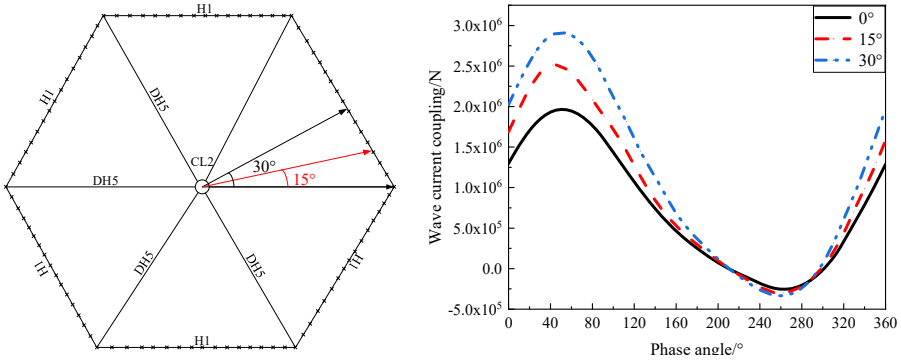

Fig. 6. Wind, wave and current coupling force phase angle relationship.

2. DMF Numerical Model

A hydrodynamic numerical model of the DMF platform has been developed utilizing the finite element simulation approach, demonstrating its feasibility. To enhance computational accuracy and streamline the analytical process, rigid constraints were applied to the overall model, which exert minimal influence on the dynamic response characteristics of the floating structures. Given the relationship between the dimensions of offshore floating structures and the wavelength, the DMF floats were represented using a surface element modeling technique appropriate for large-scale structures. Conversely, the DMF cross braces, classified as smaller-scale components, were modeled employing the Morrison element method.

2.1. Environmental parameters

Environmental parameters for the DMF were established based on prevailing sea conditions and the maximum wind speeds that offshore wind turbine blades can endure. Two environmental scenarios were considered: normal operating conditions and extreme sea states. Simulation tests conducted under both scenarios facilitated a comprehensive evaluation of the system's stability and safety parameters, ensuring resilience against the most severe environmental conditions anticipated during operational periods. The selection of environmental parameters was guided by standards from both the International Electrotechnical Commission (IEC) and the National Renewable Energy Laboratory (NREL), as detailed in Table 2.

Table 2. Environmental parameters

Parameters	Water depth/m	Cycle/s	Wave height/m	Wind spectrum	Current speed/m/s	Wind speed/m/s
Rated	100	11.3	5.49	NPD	0.39	11.4
Extreme		15.8	10.6		2.3	56.3

2.1.1. Hydrodynamic model

Fig. 5 illustrates the numerical model of the DMF platform system. A static water surface model and a maximum inclination response amplitude model under dynamic wave loading conditions were developed. The coordinate system is defined such that the x-axis aligns positively with the wind direction, the water surface lies within the x0y plane, and the z-axis is oriented perpendicular to the water surface, pointing upwards. The model employs A36 steel as the construction material, chosen for its suitability in large-scale offshore structures and its capacity to withstand a maximum yield strength of 450 MPa. The Poisson's ratio of the material is specified as 0.3. The DMF platform features a water column height of 10 m and a submerged wet surface depth of 35 m, classifying it as a semi-submersible structure.

2.2. Wind Turbine Wake Simulation

2.2.1. Single wind turbine aerodynamic simulation

The inlet wind speed was set to 11.4 m/s to satisfy the maximum power wind speed criteria outlined in Table 2. The rotor sweep radius was 59.8 m, and the wind field was modeled as a two-dimensional domain measuring 500 m by 200 m. The wake dynamics of a single wind turbine are illustrated in Fig. 7.

Simulation results indicate that under stable wind field conditions, the wake variations of the wind turbine conform to the pattern described by Eq. (3), thereby validating the accuracy of the proposed model.

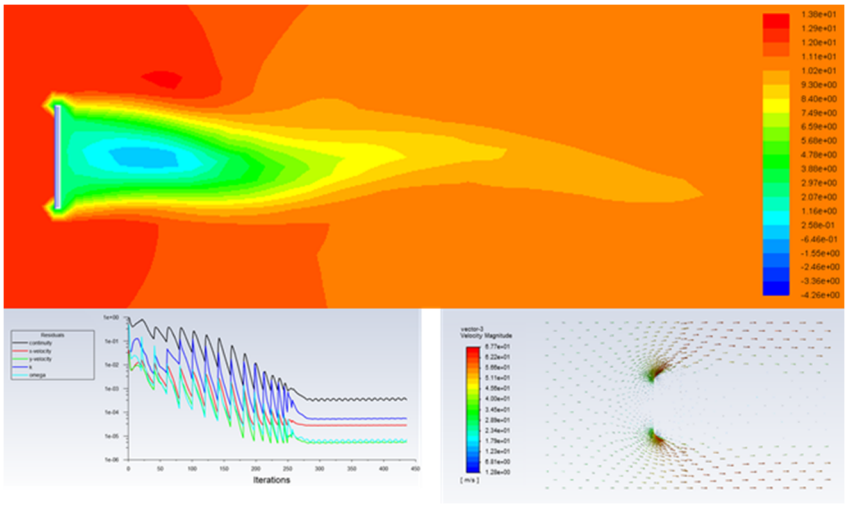

Fig. 7. Single wind turbine wake results.

2.2.2. Aerodynamic simulation of multiple wind turbines

A wind farm comprising multiple wind turbines was simulated with an inlet wind speed of 11.4 m/s. The wake variation patterns for each turbine are presented in Fig. 8. The rotor sweep radius remained 59.8 m, and the wind field was expanded to a two-dimensional area of 500 m by 500 m.

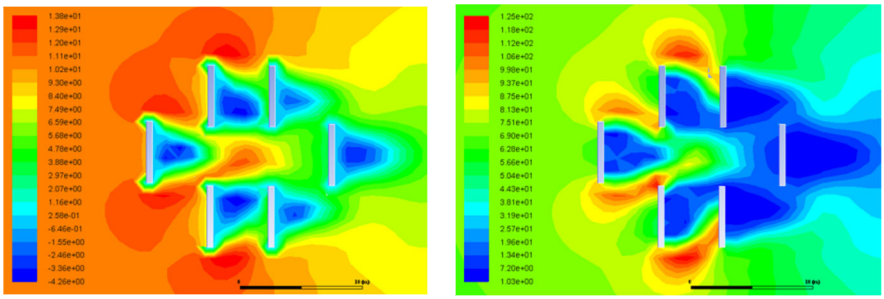

(a) (b)

Fig. 8. Multiple wind turbine wake results. (a) Wind speed; (b) Wind pressure.

Fig. 8(a) demonstrates a reduction in wind speed at the downstream turbines attributable to the wake effects generated by upstream turbines, consistent with the wake attenuation laws for multiple wind turbines. Additionally, the increased wind pressure observed at the downstream turbines aligns with established multi-turbine wake load principles, offering valuable insights for the design of novel multi-wind integrated structures.

Wind, wave, and current loads constitute critical environmental factors influencing the stability of offshore floating platforms. Under the specified test conditions, regular wind, wave, and current profiles were employed, with varying heights applied along the positive x-axis direction. The study investigated the variation in the Dynamic Motion Frequency (DMF) pitch response amplitude, excluding the influence of wind and ocean currents. The principal dynamic responses of the DMF system under the selected regular environmental loads are depicted in Fig. 9. The numerical results exhibit strong agreement with experimental data, although the numerical model slightly underestimates the dynamic response of the DMF. This discrepancy is primarily attributed to the combined effects of viscous damping and eddy currents present in the small-scale experimental setup, which amplify the structural motion response.

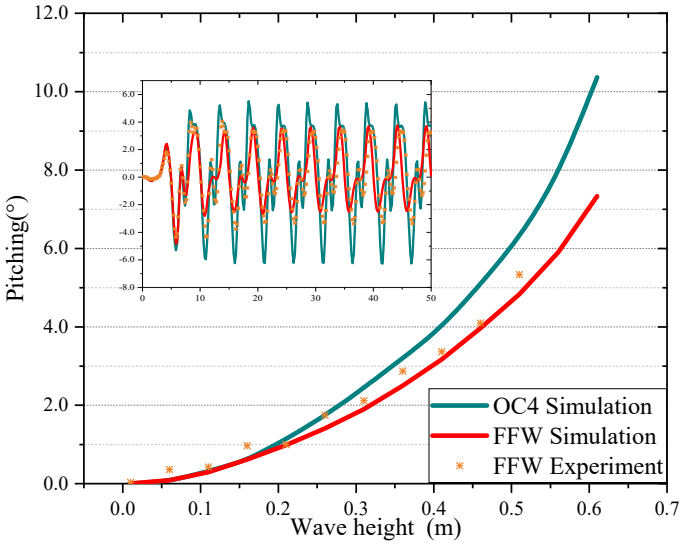

Fig. 9. DMF wind, wave and current height and pitch results.

Fig. 9 shows that the variation of hydrodynamic response amplitude of DMF multi wind turbine combination system and traditional OC4 single wind turbine model is based on different environmental load parameters. Moreover, the rate of increase in pitch amplitude (slope) becomes steeper with larger wind, wave, and current heights. Across the entire design range of these environmental conditions, the pitch response amplitude of the DMF multi wind turbine combination system is lower than the traditional OC4 single wind turbine model. The arrow-indicated curve in Fig. 9 further demonstrates that, under sinusoidal wind, wave, and current conditions with a height of 0.5 m, the pitch response amplitudes of both DMF and OC4 follow a sinusoidal pattern. Notably, the DMF's pitch amplitude is marginally smaller than that of the OC4, and this disparity increases with rising wind, wave, and current heights, indicating enhanced adaptability of the DMF in harsh marine environments relative to the OC4.

3. Small Scale Model Test

To investigate the more realistic motion response characteristics of the DMF design, a model flume test was conducted. Given the large scale and extensive span of the DMF structure, constructing a full-scale physical model remains challenging at this stage. Consequently, this study employed a similarity ratio of 1:200 to create an equivalent scaled model, thereby simplifying the experimental implementation. Utilizing push plate equipment and blast force generators, simulated sea states with varying wind, wave, and current heights, periods, current velocities, and wind speeds were generated. The integrated device's motion characteristics under these diverse environmental conditions were obtained through the model tests. Hydrodynamic motion response data of DMF were measured using a tension sensing system and tilt sensors, enabling the evaluation of the hydrodynamic performance of the scaled model through small-scale testing methods.

3.1. Small Scale Model Parameters

To ensure that the test data accurately represent real-world conditions, it is essential that the physical properties of the model closely resemble those of the actual object. This study conducts prototype testing of a water tank model primarily influenced by hydrodynamic forces. The model fabrication aims to approximate the Reynolds number similarity as closely as possible. The scaling is performed according to a predetermined scale ratio, with the test model constructed at a 1:200 scale. Certain physical parameters are proportionally converted, and the relationships between the model`s physical parameters in Table 3.

Table 3. Physical Parameters

Parameter	Relation	Test	Actual	Ratio
Quality /kg	∇_s/∇_m	54.375	4.35×10^8	λ^3
Wind, wave and current height /m	H_s/H_m	0.027	5.49	λ_b
Period/s	T_s/T_m	0.806	11.3	$\lambda^{1/2}$
Velocity /m/s	v_s/v_m	0.81	11.4	$\lambda^{1/2}$
Moment of inertia	I_s/I_m	30.59, 30.59, 12.78	9.788×10^{12}, 9.788×10^{12}, 4.089×10^{12}	λ^5

3.2. DMF Testing Model

The fabrication and development of small-scale DMF model prototypes must rigorously adhere to the principles of geometric and dynamic similarity. This adherence is critical for accurately evaluating the performance of small-scale model tests. To maintain consistency in both geometric proportions and mass similarity, the model is constructed using fiberglass material. Additionally, to ensure alignment of the waterline surfaces between the original full-scale model and the scaled-down prototype, a ballast weight is affixed to the base of the DMF float to achieve buoyant equilibrium. Fig. 10 illustrates the visual representation of the DMF small-scale model prototype.

Fig. 10. Experimental equipment and prototypes.

3.3. Test Procedure

The DMF system for generating wind, waves, and currents is installed at the upstream end of the tank, while a corresponding system for mitigating wind, wave, and current reflections is positioned at the downstream end to minimize reflective interference. The wind, wave, and current generation apparatus consists of a hollow box plate capable of producing waves with periods ranging from 0.5 s to 5 s and frequencies between 0.6 Hz and 2 Hz. At a standard water depth of 1 m, this system can generate waves with heights up to 0.35 m and wavelengths spanning from 0.6 m to 20 m. During testing, the model was placed near the downstream to ensure the precision of the wind, wave, and current conditions, as well as to facilitate sensor placement and data acquisition.

Fig. 11 illustrates the six mooring lines of the DMF system alongside the hydrodynamic response characteristics. The amplitude of the oscillatory response was measured using an inclinometer and a high-speed camera, while mooring line tensions were recorded via tension sensors.

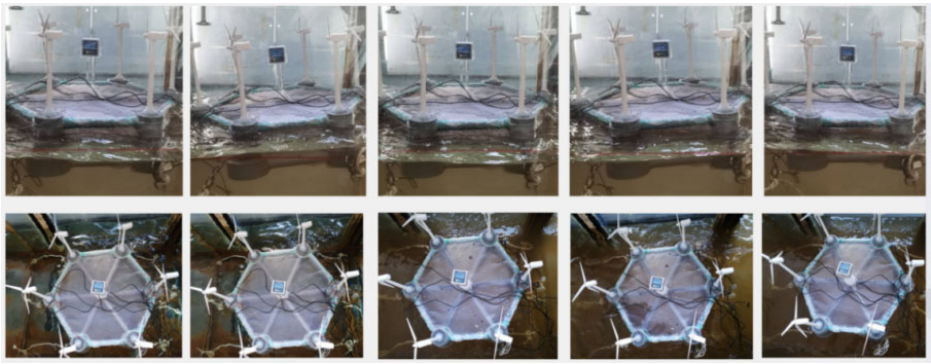

Fig. 11. Time domain motion variation law.

The DMF represents an innovative offshore floating structure design for which existing research data are insufficient for direct comparison or validation. Consequently, this study developed an identical scale model for both hydrodynamic testing and numerical simulation. The accuracy of the DMF small-scale model was assessed by comparing experimental and simulation results. The research primarily focused on simulating and experimentally investigating the six degrees of freedom hydrostatic damping and the operational response under combined wind, wave, and current conditions.

Under consistent wind, wave, and mooring parameters, the six degrees of freedom motion responses and mechanical behavior of the floating structure were obtained, as depicted in Fig. 12.

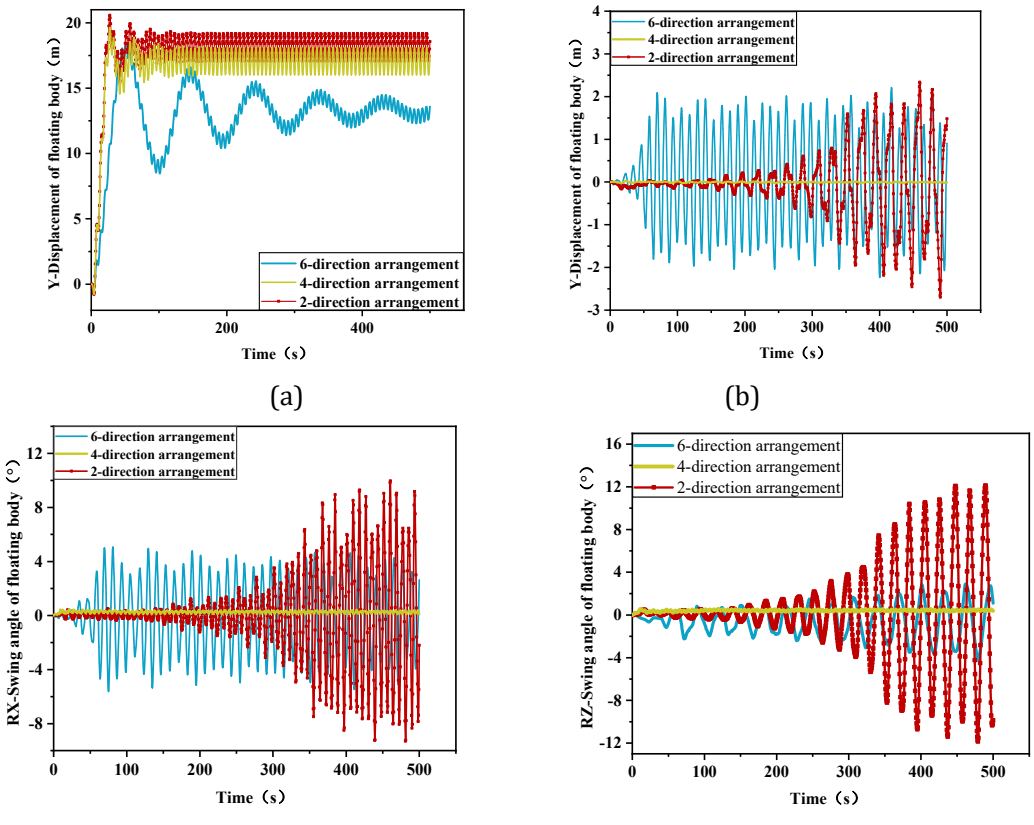

Fig. 12. Comparison of motion response. (a) Catenary sway response; (b) Tensioned surge response; (c) Response of tensioned roll; (d) Catenary yaw response.

The dynamic response outcomes of tension-type and catenary-type mooring systems with multiple degrees of freedom were compared to assessing the superiority of the optimized mooring configuration. Traditional catenary mooring exhibits poor stability in the surge direction. As illustrated in Fig. 12(a), the two-way mooring arrangement demonstrates a shorter duration to reach stable oscillation and superior stability performance compared to the conventional six-way configuration. Fig. 12(b), (c), and (d) reveal that the sway motion amplitude remains minimal during the initial phase of the two-way arrangement time-domain simulation but gradually increases in the later stages, indicating a deterioration in stability. It is inferred that optimal mooring performance is achieved when the mooring lines with significant tension constraints are arranged in a balanced manner and oriented perpendicularly to the prevailing wind, wave, and current loads.

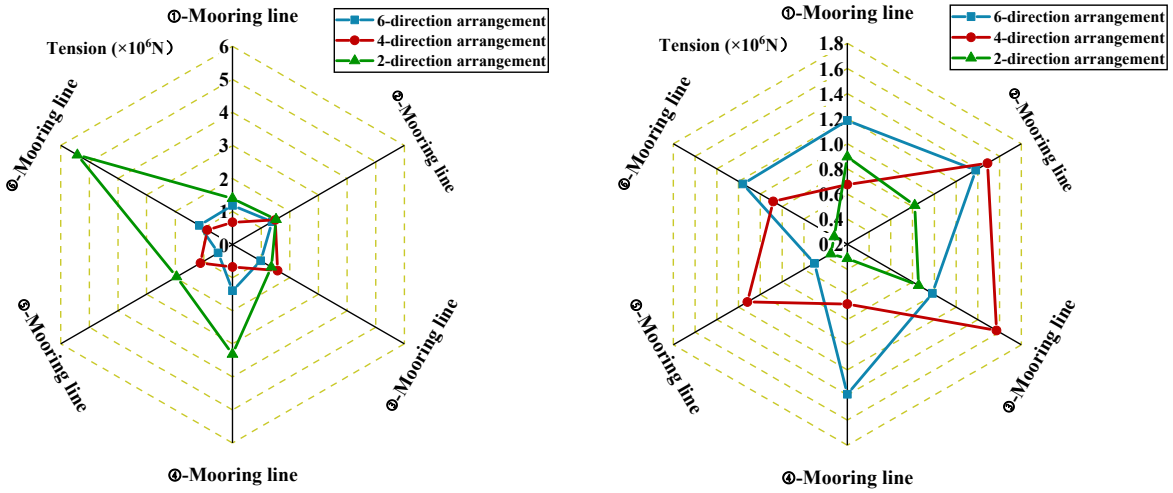

(a) (b)

Fig. 13. Comparison of tension extremum. (a) Load of catenary; (b) load of tension.

Regarding mooring tension variations, Fig. 13(a) indicates that the maximum tension values in the optimized catenary mooring with two- and four-direction arrangements outperform those of the six-way arrangement. Moreover, the tension distribution in the two optimized configurations is more uniform, resulting in enhanced control effectiveness. Fig. 13(b) shows negligible changes in the tension values of each cable in the tensioned mooring system before and after optimization. This observation is attributed to the strong self-restraint characteristics of tensioned mooring cables and their significant sensitivity to floating body oscillations, which limit tension variation across different arrangement schemes.

In this study, the simulation environment we set up referred to the existing OC4 platform testing environment load. DMF is a combination of six wind turbines. Therefore, special attention should be paid to the influence of multiple wind turbine wake effects in the setting of aerodynamic loads. The aerodynamic load of a single wind turbine on the OC4 platform is 800 kN. By applying an initial aerodynamic load on the DMF multi wind turbine platform, the six degree of freedom dynamic response characteristics of DMF are analyzed. As shown in Fig. 13.

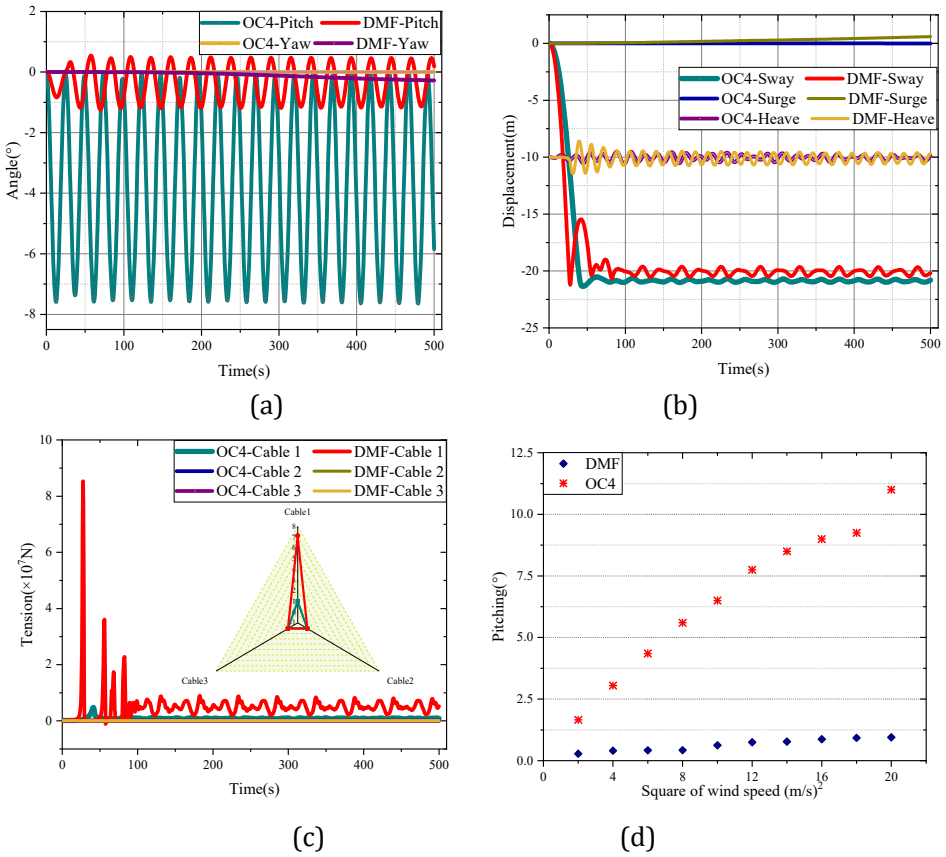

Fig. 14 Motion response. (a) Rocking time domain; (b) Oscillation time domain; (c) Mooring tension; (d) Wind speed and pitch.

Fig. 14 (a) shows that the DMF multi wind turbine system has better dynamic stability compared to the OC4 single wind turbine system. The maximum roll of DMF is −1.2°. The maximum roll of OC4 is −7.8°. This indicates that the dynamic response stability of DMF has been improved by 76%. Additionally, Fig. 20(b) reveals a significant difference in the amplitude of sway motion responses between the two models. During the interval from 0 s to 100 s, the horizontal displacement of both DMF and OC4 foundations approaches −23 m, influenced by the initial horizontal load and mooring forces. Notably, the DMF foundation exhibits a return displacement between 25 s and 60 s that is approximately three times greater than that of OC4, attributable to a sixfold difference in wind force along the D horizontal direction. The test results confirmed the variation and corresponding relationship between the load and displacement of offshore floating structures. The time-domain variation law of the tension load of the DMF mooring system shown in Fig. 14(c). Given that pitch exhibits the most significant variation among the six degrees of freedom, Fig. 14(d) further examines the effect of varying wind speeds on the pitch angles of DMF and OC4. Both models display an increasing trend in pitch angle with rising wind speed; however, the magnitude of increase in the DMF is substantially less than that observed in OC4, thereby reinforcing the superior stability and performance of the DMF in pitch response.

4. Conclusion

This study proposes and investigates a novel integrated development system combining fishery and wind power, contextualized within the current advancements in marine renewable energy and three-dimensional technological applications. The proposed scheme effectively addresses issues related to the instability of offshore wind power installations and cage aquaculture structures, as well as the suboptimal utilization of

marine spatial energy resources. Furthermore, it enhances the system's resilience to extreme offshore wind and wave load conditions.

Utilizing finite element numerical simulation techniques, modal analysis and transient dynamic analysis were conducted on the DMF system structure. The maximum wave and current loads acting on the diagonal brace members and the upper and lower crossbars of the cage structure were determined through the phase angle search principle. Results indicate that significant stress fluctuations in the cage structure occur primarily under initial wave and current loading. It was demonstrated that transient dynamic stresses substantially exceed those predicted by static material analysis. Moreover, the findings from both modal and transient dynamic analyses satisfy the safety requirements stipulated by relevant structural codes. These outcomes provide valuable theoretical frameworks and methodological approaches for the research and development of novel offshore engineering equipment.

The application of a mesh grouping method allowed for the simplification of complex computational scenarios, thereby enhancing the efficiency of finite element analyses. This approach maintained the integrity of total mass and horizontal load parameters before and after mesh clustering during the simplification process. Numerical simulations confirmed that the mechanical characteristics were accurately represented, supporting the suitability of the mesh grouping method for evaluating the bearing capacity of large-scale structural equipment.

Through comparative analysis of numerical simulation and experimental testing, it has been determined that DMF has improved hydrodynamic stability by 47% on traditional floating platform foundations. This further validates the superiority and feasibility of the DMF system proposed.

Despite these advancements, numerous challenges remain regarding the practical feasibility of integrated wind power and fishery systems. Future research should focus on developing a robust framework for real-world implementation, particularly emphasizing the optimization of power generation efficiency and the layout configuration of six wind turbines. Additionally, long-term fatigue analysis and its implications must be addressed. These considerations are essential for subsequent investigations in this domain.

Nomenclature

DMF = Dot Matrix Floating wind turbine

v_n = downstream wind velocity (m/s)

v_0 = initial wind speed (m/s)

C_M = mass factor

C_{dt} = tangential flow resistance

C_{dn} = normal flow resistance

F_c = current load (N)

S_{ij} = waterline cross-section (m^2)

R_{Di} = horizontal spacing size (m)

Conflict of Interest

The authors declare that they have no known competing financial interests or personal relationships that could have appeared to influence the work reported in this paper.

Author Contributions

Jiangfeng Zhu: Conceptualization, Methodology, Software, Writing—original draft. Funding acquisition, Supervision. Qian Zhao: Validation, Writing—review & editing. All authors had approved the final version.

Acknowledgement

The support for this research is gratefully acknowledged to the Qingdao Huanghai University Doctoral Professor Research Project—Research on dynamic characteristics of offshore floating multi wind power combination platform based on flexible constraints (2025boshi01) and China University of Petroleum (East China) marine engineering experiment center and Qingdao West Coast science and technology innovation project "Research on Key Technologies of marine fishery electricity integrated development system (2019-8)".

Reference

[1] Liang, J., Huang, J., & Huang, H. (2021). SWOT analysis on the Belt and Road innovation cooperation between Guangdong and Brazil. *Journal of Electronic Research and Application*, *4(6)*, 119–126. https://doi.org/10.26689/JERA.V4I6.1752

[2] Chao, H., Cheng, Z., Hai-Jun, G., *et al.* (2017). Fast startup of semi-pilot-scale anaerobic digestion of food waste acid hydrolysate for biogas production. *Journal of Agricultural and Food Chemistry*, *65(51)*, 11237–11242. https://doi.org/10.1021/acs.jafc.7b04005

[3] Jiang, J., Liang, C., Chen, Y., *et al.* (2025). The influence of process parameters on the density, microstructure, and mechanical properties of TA15 titanium alloy fabricated by selective laser melting. *Metals*, *15(3)*, 233. https://doi.org/10.3390/MET15030233

[4] Wang, W., Li, H., Yang, Y., *et al.* (2025). Stability analysis of semi-submersible floating wind turbines based on gyro-turbine coupled dynamics model. *Frontiers in Marine Science*, *12*, 1597408. https://doi.org/10.3389/FMARS.2025.1597408

[5] Chang, C., Song, M., Liu, F., *et al.* (2025). Structural deformation dynamic simulation of weft knitted fabric basic stitch. *The Journal of the Textile Institute*, *116(3)*, 389–398. https://doi.org/10.1080/00405000.2024.2337316

[6] Chen, M., Shang, R., Sberna, M. P., *et al.* (2020). Highly permeable silicon carbide-alumina ultrafiltration membranes for oil-in-water filtration produced with low-pressure chemical vapor deposition. *Separation and Purification Technology*, *253*, 117496. https://doi.org/10.1016/j.seppur.2020.117496

[7] Xiao, S., Zhang, H., Wei, Y., *et al.* (2025). Analysis of the overall structural strength and optimization recommendations for ultra-large container ships based on the improved equivalent design wave method. *Mechanics of Advanced Materials and Structures*, *32(16)*, 4001–4011. https://doi.org/10.1080/15376494.2024.2400239

[8] Dutta, S. C., & Roy, R. (2002). A critical review on idealization and modeling for interaction among soil–foundation–structure system. *Computers and Structures*, *80(20–21)*, 1579–1594. https://doi.org/10.1016/S0045-7949(02)00115-3

[9] Vamshinath, K., Niteesh Kumar, N., Tarun Kumar, R., Nagaraju, D. S., Sateesh, N., Subbaiah, R. (2022). Analysis of the effect of the process parameters on the mechanical strength of 3D printed and adhesively bonded PETG single lap joint. *Materials Today: Proceedings*, *62(P6)*, 4509–4514. https://doi.org/10.1016/J.MATPR.2022.04.950

[10] Lupton, R. C., Langley, R. S. (2020). Harmonic linearisation of aerodynamic loads in a frequency-domain model of a floating wind turbine. *Wind Energy*, *24(8)*, 833–856. https://doi.org/10.1002/WE.2605

[11] Mahfouz, M. Y., Faerron-Guzmán, R., Müller, K., Lemmer, F., Cheng, P. W. (2020). Validation of drift motions for a semi-submersible floating wind turbine and associated challenges. *Journal of Physics: Conference Series*, *1669(1)*, 012011. https://doi.org/10.1088/1742-6596/1669/1/012011

[12] Wen, B., Li, Z., Jiang, Z., *et al.* (2020). Experimental study on the tower loading characteristics of a floating wind turbine based on wave basin model tests. *Journal of Wind Engineering & Industrial Aerodynamics*,

207, 104390. https://doi.org/10.1016/j.jweia.2020.104390

[13] Pivert, L. F., Roberts, A., Santander, L. A., *et al.* (2025). Data driven multi-objective optimization of the scheduling for towing a floating offshore wind turbine between assembly port and installation location throughout a year. *Applied Ocean Research*, *157*, 104492. https://doi.org/10.1016/J.APOR.2025.104492

[14] Li, Y., Yin, W., Leng, S., *et al.* (2025). Dynamic analysis of a spar-type floating offshore wind turbine under extreme operation gust. *Sustainability*, *17(12)*, 5655. https://doi.org/10.3390/SU17125655

[15] Yue, M., Liu, Q., Li, C., *et al.* (2020). Effects of heave plate on dynamic response of floating wind turbine spar platform under the coupling effect of wind and wave. *Ocean Engineering*, *201*, 107103. https://doi.org/10.1016/j.oceaneng.2020.107103

[16] Wise, S. A., & Bachynski, E. E. (2020). Wake meandering effects on floating wind turbines. *Wind Energy*, *23(5)*, 1266–1285. https://doi.org/10.1002/we.2485

[17] Simon, B., Guilherme, V., Sebastien, G., *et al.* (2020). Investigation of a semi-submersible floating wind turbine in surge decay using CFD. *Ship Technology Research*, *67(1)*, 2–14. https://doi.org/10.1080/09377255.2018.1555987

[18] He, W., Xiang, W., He, X., *et al.* (2020). Boundary vibration control of a floating wind turbine system with mooring lines. *Control Engineering Practice*, *101*, 104423. https://doi.org/10.1016/j.conengprac.2020.104423

[19] Shuchuang, D., Xinxing, Y., & Fuxiang, H. (2021). Experimental investigation on the fluid–structure interaction of a flexible net cage used to farm Pacific bluefin tuna (*Thunnus orientalis*). *Ocean Engineering*, *226*, 108872. https://doi.org/10.1016/J.OCEANENG.2021.108872

[20] Tiao-Jian, X., Guo-Hai, D., Ming-Fu, T., *et al.* (2021). Experimental analysis of hydrodynamic forces on net panel in extreme waves. *Applied Ocean Research*, *107*, 102495. https://doi.org/10.1016/J.APOR.2020.102495